

Reducing vortex density in superconductors using the ‘ratchet effect’

C.-S. Lee*, B. Jankó†, I. Derényi‡ & A.-L. Barabási*

* Department of Physics, University of Notre Dame, Notre Dame, Indiana 46556, USA

† Materials Science Division, Argonne National Laboratory, 9700 South Cass Avenue, Argonne, Illinois 60439, USA

‡ Department of Surgery, MC 6035, University of Chicago, 5841 South Maryland Avenue, Chicago, Illinois 60637, USA

A serious obstacle impeding the application of low- and high-temperature superconductor devices is the presence of trapped magnetic flux^{1,2}: flux lines or vortices can be induced by fields as small as the Earth’s magnetic field. Once present, vortices dissipate energy and generate internal noise, limiting the operation of numerous superconducting devices^{2,3}. Methods used to overcome this difficulty include the pinning of vortices by the incorporation of impurities and defects⁴, the construction of flux ‘dams’⁵, slots and holes⁶, and magnetic shields^{2,3} which block the penetration of new flux lines in the bulk of the superconductor or reduce the magnetic field in the immediate vicinity of the superconducting device. The most desirable method would be to remove the vortices from the bulk of the superconductor, but there was hitherto no known phenomenon that could form the basis for such a process. Here we show that the application of an alternating current to a superconductor patterned with an asymmetric pinning potential can induce vortex motion whose direction is determined only by the asymmetry of the pattern. The mechanism responsible for this phenomenon is the so-called ‘ratchet effect’^{7–10}, and its working principle applies to both low- and high-temperature superconductors. We demonstrate theoretically that, with an appropriate choice of pinning potential, the ratchet effect can be used to remove vortices from low-temperature superconductors in the parameter range required for various applications.

We consider a type II superconductor film of the geometry shown in Fig. 1a, placed in an external magnetic field H . The super-

conductor is patterned with a pinning potential $U(x, y) = U(x)$ which is periodic with period l along the x direction, has an asymmetric shape within one period, and is translationally invariant along the y direction of the sample. The simplest example of an asymmetric periodic potential, obtained for example by varying the sample thickness, is the asymmetric sawtooth potential (Fig. 1b). In the presence of a current with density J flowing along the y axis the vortices move with the velocity

$$v = (f_L + f_{vv} + f_u)/\eta \quad (1)$$

where $f_L = (J \times \hat{h})\Phi_0 d/c$ is the Lorentz force moving the vortices transverse to the current, c is the velocity of light in vacuum, \hat{h} is the unit vector pointing in the direction of the external magnetic field H , $f_u = -(dU/dx)\hat{x}$ is the force generated by the periodic potential, f_{vv} is the repulsive vortex–vortex interaction, $\Phi_0 = 2.07 \times 10^{-7}$ G cm² is the flux quantum, η is the viscous drag coefficient, and d is the length of the vortices (that is, the thickness of the sample).

When a direct current flows along the positive y direction, the Lorentz force moves the vortices along the positive x direction with velocity v_+ . Reversing the current reverses the direction of the vortex velocity, but its magnitude, $|v_-|$, due to the asymmetry of the potential, is different from v_+ . For the sawtooth potential shown in Fig. 1b, the vortex velocity is higher when the vortex is driven to the right, than when it is driven to the left ($v_+ > |v_-|$). As a consequence the application of an alternating current (which is the consecutive application of direct and reverse currents with density J) results in a net velocity $v = (v_+ + v_-)/2$ to the right in Fig. 1b. This net velocity induced by the combination of an asymmetric potential and an a.c. driving force is called ratchet velocity^{7–10}. The ratchet velocity for the case of low vortex density (when vortex–vortex interactions are neglected) can be calculated analytically. Denoting the period of the alternating current by T , the ratchet velocity of the vortices in the $T \rightarrow \infty$ limit is given by the expression

$$v = \begin{cases} 0 & \text{if } f_L < f_1 \\ \frac{1}{2\eta} \frac{(f_1 + f_2)(f_L - f_1)}{f_L + f_2 - f_1} & \text{if } f_1 < f_L < f_2 \\ \frac{1}{\eta} \frac{f_1 f_2 (f_2 - f_1)}{f_2^2 - (f_2 - f_1)^2} & \text{if } f_2 < f_L \end{cases} \quad (2)$$

where $f_1 = \Delta U/l_1$ and $f_2 = \Delta U/l_2$ are the magnitudes of the forces generated by the ratchet potential on the facets of length l_1 and l_2 , respectively (Fig. 1c), ΔU is the energy difference between the

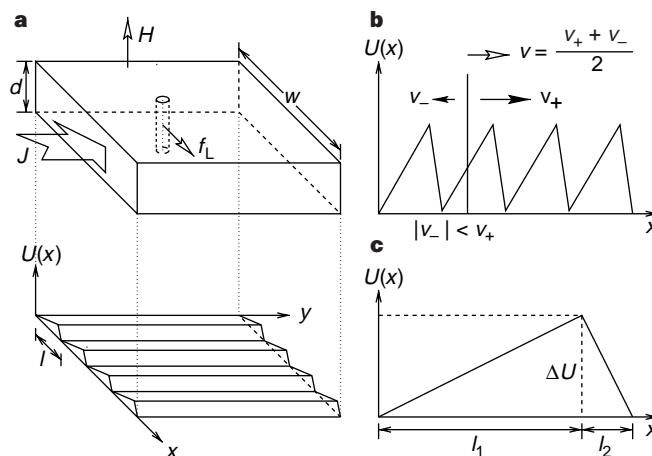


Figure 1 Patterning of a superconductor with an asymmetric potential. **a**, Diagram of a superconductor in the presence of an external magnetic field H . A direct current with density J flowing along the y direction (indicated by the large arrow) induces a Lorentz force f_L that moves the vortex in the x direction. The superconductor is patterned with a pinning potential $U(x, y) = U(x)$, whose shape is shown in the lower panel. The potential is periodic and asymmetric

along the x direction, and is translationally invariant along y . **b**, The pinning potential $U(x)$ along the superconductor’s cross-section. The solid arrows indicate the vortex velocity v_+ (v_-) induced by a direct $+J$ (reversed $-J$) current. The average, $v = (v_+ + v_-)/2$, is the ratchet velocity of the vortex, obtained when an alternating current is applied. **c**, The parameters characterizing a single tooth of the asymmetric potential.

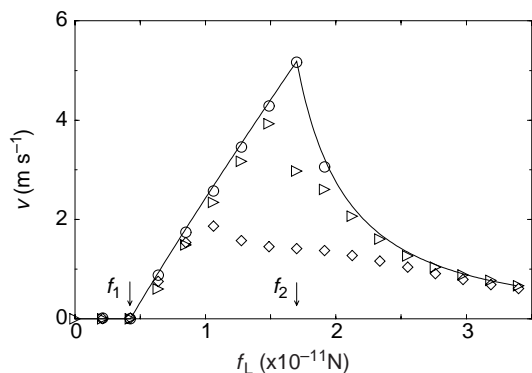


Figure 2 Ratchet velocity of the vortices as a function of the amplitude of the driving force f_L . The thick solid line corresponds to the analytical result (equation (2)) for a single vortex line. The symbols are the result of the numerical simulations for multiple vortices. The simulations were done using the model developed by Nori and collaborators^{20–22}, assuming that the rigid vortices are point-like objects moving in the x - y plane. At time zero the vortices are positioned randomly in the superconductor with a density ρ_0 and they move with velocity given by equation (1). The vortex–vortex interaction between two vortices at position \mathbf{r}_i and \mathbf{r}_j is modelled using $\mathbf{f}_{ij} = \Phi_0^2 d / (8\eta^2 \lambda^3) \mathcal{K}_1((\mathbf{r}_i - \mathbf{r}_j) / \lambda) \hat{\mathbf{r}}_{ij}$, where $\hat{\mathbf{r}}_{ij} = (\mathbf{r}_i - \mathbf{r}_j) / |\mathbf{r}_i - \mathbf{r}_j|$. Here the modified Bessel function \mathcal{K}_1 is cut off beyond the distance $r = 25\lambda$, where λ is the penetration depth (for Nb $\lambda = 45$ nm at $T = 0$). The force f generated by the sawtooth pinning potential shown in Fig. 1 is equal to f_1 when $kl < x < kl + l_1$, and f_2 when $kl + l_1 < x < (k+1)l$, where $k = 0, 1, \dots, N-1$. We choose $l_1 = 20\lambda = 0.9 \mu\text{m}$, $l_2 = 5\lambda = 0.225 \mu\text{m}$, $l = l_1 + l_2$ and $N = 10$, giving for the total width of the sample $w = 11.25 \mu\text{m}$. Its length (along the y direction) is set to $12 \mu\text{m}$. The sample has periodic boundary conditions in both the x and y direction. The Lorentz force due to the alternating current is equal to $+f_L$ for $T/2$ time, and $-f_L$ for $T/2$ using $T = 0.3 \mu\text{s}$. We considered the simplest case, in which the potential is induced by thickness variations of a Nb superconductor thin film of thickness d , that is, the superconductor thickness, $d + h(x)$, changes along the x direction, following a sawtooth pattern. The pinning energy acting on the vortices is given by $U(x) = (d + h(x))\epsilon_0$, where ϵ_0 is the line energy of the vortex per unit length. Thus the magnitudes of the forces acting on the vortices are $f_1 = \epsilon_0 \Delta h / l_1$ and $f_2 = \epsilon_0 \Delta h / l_2$ for the two facets of the Δh high teeth (Fig. 1c), and we choose $\Delta h = l_2$. For Nb we have $\epsilon_0 = 1.7 \times 10^{-11}$ N, the viscosity per unit length is $\eta_0 = 7 \times 10^{-6}$ N s m^{-2} , yielding $\eta = \eta_0 d = 1.4 \times 10^{-12}$ N s m^{-1} for a $d = 2,000 \text{ \AA}$ -thick film. The total number of vortices in the simulation were $n = 5$ (open circles), $n = 250$ (open triangles) and $n = 500$ (open diamonds) corresponding to a magnetic field in the sample of about 0.7 G, 35 G and 70 G, respectively.

maximum and the minimum of the potential, and $f_L = |f_L| = J\Phi_0 d/c$.

Because vortex–vortex interactions play an important role for high magnetic fields, we have performed molecular-dynamics simulations to determine the ratchet velocity for a collection of vortices. As Fig. 2 demonstrates, we find that for low vortex densities the numerical results follow closely the analytical prediction (equation (2)), and the magnitude of the ratchet velocity decreases with increasing vortex density. The vortex densities used in the simulations correspond to an internal magnetic field of about 0.7, 35 and 70 G, covering a wide range of magnetic fields. An important question for applications is if the ratchet velocity (equation (2)) is large enough to induce observable vortex motion at experimentally relevant timescales. To address this issue in Fig. 2 we plotted v for niobium, a typical low-temperature superconductor used in a wide range of devices, for which the potential $U(x)$ is induced by thickness variations of the superconductor. The details of the model are described in Fig. 2 legend. As the figure indicates, the maximum ratchet velocity (5.2 m s^{-1}) is high enough to move a vortex across the width of a typical sample (a few micrometres; ref. 3) in a few microseconds. Furthermore, increasing the vortex density by two orders of magnitude decreases the vortex velocity by only a factor of three.

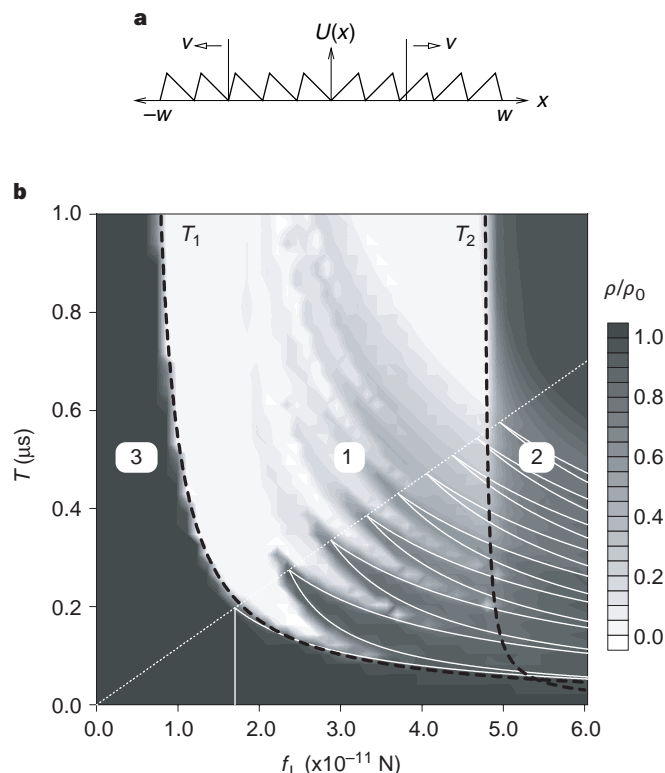


Figure 3 Removing vortices from a superconductor using an asymmetric potential. **a**, The potential necessary to remove vortices from the superconductor. Using the simulation method described in Fig. 2 legend, we investigated a system consisting of $N = 5$ teeth oriented to the left and the same number oriented to the right, as shown in the figure, the parameters of each tooth being identical to that described in Fig. 1c. To mimic the pressure generated by the external magnetic field, which acts to push vortices into the sample, on the two sides we attached two reservoirs, which have a constant vortex density ρ_0 at all times. Thus, vortices can leave the sample for the reservoir, or new vortices can enter from the reservoir. In thin superconducting films, due to the Meissner current, there is a geometrical barrier that acts to trap the vortices inside the sample²³. As most applications of superconductors involve thin films, we included in the simulations this geometrical barrier, which creates a force $f_{in}(x) = -(H\Phi_0/2\pi)\kappa l\sqrt{w^2 - x^2}$ for $-w + d/2 < x < w - d/2$, and $f_{edge} = 2\epsilon_0 - (H\Phi_0/2\pi)\sqrt{4w/d - 1}$ for $x > w - d/2$, and $-f_{edge}$ for $x < -w + d/2$. Thus the geometrical barrier opposes the entry of the vortices at the edge of the superconductor, but once they move inside, it moves them towards the centre of the superconductor. For successful vortex removal, the ratchet effect has to be strong enough to move the vortices against $f_{in}(x)$. **b**, The (f_L, T) diagram describing the effectiveness of the ratchet effect as a function of the parameters characterizing the driving current, f_L . The grey scale corresponds to the relative vortex density ρ/ρ_0 , where ρ_0 is the initial vortex density corresponding to $H = 1$ G and ρ is the final vortex density after the application of the alternating current. As the grey shading indicates, there is a region where vortex removal is complete, the vortex density being equal to zero. The dashed black lines correspond to the T_1 and T_2 boundaries, which are calculated analytically (see text) and separate the three main regimes: regime 1, complete vortex removal in much of the regime, $\rho = 0$; regime 2, partial vortex removal, $0 \leq \rho < \rho_0$; and regime 3, no change in the vortex density, $\rho = \rho_0$. The thin solid white lines denote the boundaries of the regions where vortex trapping occurs due to periodic orbits. These boundaries correctly reflect the structure of the fingers, but slightly deviate from the results of the numerical simulation, because the analytical calculation assumed an array of identical teeth.

Next, we discuss a potentially useful application of the ratchet effect by demonstrating that it could be used to drive vortices out of a superconductor. We consider a superconducting film that is patterned with two arrays of the ratchet potential oriented in opposite directions (Fig. 3a). During the application of the alternating current, the asymmetry of the potential in the right half

moves the vortices in that region to the right, while vortices in the left half move to the left. Thus the vortices drift towards the closest edge of the sample, decreasing the vortex density in the bulk of the film. We performed numerical simulations to quantitatively characterize this effect (details and the parameters are described in Fig. 3 legend). In Fig. 3b we summarize the effectiveness of vortex removal by plotting the reduced vortex density inside the film as a function of the Lorentz force f_L and the period T of the current. There is a well defined region where the vortex density drops to zero inside the sample, indicating that the vortices are completely removed from the bulk of the sample. Outside this region, we observe either a partial removal of the vortices or the alternating current has no effect on the vortex density.

The (f_L, T) diagram shown in Fig. 3b has three main regimes (1, 2 and 3) separated by two boundaries. The $T_1 = 2\eta l_1 / \{f_L - [f_1 + f_{in}(-w + l_2)]\}$ phase boundary (here we assume $d/2 < l_2$, w is the width of the sample, and $f_{in}(x)$ is defined in Fig. 3 legend) provides the time needed to move the vortex all the way up on the l_1 long facet of the ratchet potential at the edge of the superconductor, that is, to remove the vortex from the superconductor. When $T < T_1$, the vortices cannot leave the superconductor. The T_2 phase boundary defined as

$$T_2 = 2\eta \left(\frac{d/2}{f_L - [f_2 + f_{edge}]} + \frac{l_2 - d/2}{f_L - [f_2 - f_{in}(-w + d/2)]} \right)$$

where f_{edge} , also defined in Fig. 3, is the time needed for a vortex to enter from the edge of the superconductor past the first potential maxima. Thus, when $T < T_2$ the vortices cannot overcome the edge of the potential barrier. These phase boundaries, calculated for non-interacting vortices, effectively determine the vortex density in the three phases. Vortex removal is most effective in regime 1, where the vortices cannot move past the first potential barrier when they try to enter the superconductor, but they get past the barriers opposing their exit from it. Thus the vortices are swept out of the superconductor by the ratchet effect, and no vortex can re-enter, leading to a vortex density $\rho = 0$. Indeed, the numerical simulations indicate complete vortex removal in much of this phase (see the contour lines in Fig. 3b). An exception is the finger structure near the crossing of the T_1 and T_2 boundaries. For fields and periods within the first finger (situated almost entirely in regime 3 in Fig. 3b), the vortex follows a periodic orbit inside a single potential well¹⁰. The subsequent fingers represent stable period orbits between two, three or more wells, respectively. As the vortices cannot escape from these orbits, they remain trapped inside the superconductor, increasing the vortex density within the fingers in the phase diagram. Figure 3b shows (as white solid lines) the analytically calculated envelopes of the regions where such trapping occurs. An important feature of the finger structure is that stable periodic orbits, which prevent vortex removal, do not exist above the line $T_{tip} = f_L 2\eta \Delta U / [f_1 f_2 (f_2 - f_1)]$ connecting the finger tips. In regime 2 vortices can enter the superconductor, but the ratchet effect is still sweeping them out; so here we expect partial removal of the vortices, the final vortex density inside the superconductor being determined by the balance of vortex nucleation rate at the edge of the sample (which depends on its surface properties) and the ratchet velocity moving them out. In regime 3 the vortices cannot leave the superconductor and new vortices cannot enter the system, thus the initial density inside the superconductor is unchanged throughout this phase ($\rho = \rho_0$).

As the forces $f_{in}(x)$ and f_{edge} depend on H , the positions of the phase boundaries T_1 and T_2 also depend on the external magnetic field. In particular, there exists a critical field H^* for complete vortex removal. For $H > H^*$, regime 1 (where vortex removal is complete) disappears, but regime 2 with partial vortex removal survives. We find that for niobium films of the geometry described in Fig. 3 we have $H^* \approx 10$ G. But as H^* is a consequence of the geometric barrier, its value can be modified by changing the aspect ratio of the film.

Furthermore, for superconductors with elliptic cross-section the geometric barrier can be eliminated¹¹, thus phase 1 with complete vortex removal could be extended to high magnetic fields as well.

Vortex removal is important for numerous applications of superconductors and can improve the functioning of several devices. An immediate application of the proposed method would be improving the operation of superconducting quantum interference devices (SQUIDs), used as sensors in a wide assortment of scientific instruments^{3,12,13}. A long-standing issue in the performance of SQUIDs is $1/f$ noise^{6,12}, arising from the activated hopping of trapped vortices¹. Reducing the vortex density in these superconductors is expected to extend the operation regime of these devices to lower frequencies.

Although over the past few years several applications of the ratchet effect have been proposed, such as separating particles^{14,15}, designing molecular motors¹⁶, smoothing surfaces¹⁷, or rectifying voltage in Josephson junctions^{18,19}, our proposal solves an acute problem of condensed-matter physics, by removing vortices from a superconductor. In contrast with most previous applications, which require the presence of thermal noise, our model is completely deterministic. Indeed, in niobium the variation in the pinning potential is $\Delta U \approx 25$ eV, which is more than 10^4 times larger than $k_B T \approx 0.8$ meV at $T_c = 9.26$ K, thus rendering thermal fluctuations irrelevant. A particularly attractive practical feature of our proposed method is that it does not require sophisticated material processing to make it work. First, it requires standard scale (micrometre scale) patterning techniques; the micrometre tooth size was chosen so that a few teeth fit on a typical SQUID, but larger feature size will also function if the period T is increased proportionally. Second, the application of an alternating current with appropriate period and intensity is rather easy to achieve. For applications where an alternating current is not desired, the vortices can be 'flushed out' before the normal operation of the device. On the other hand, if the superconducting device is driven by an alternating current (for example, radio-frequency SQUIDs, a.c. magnets, or wires carrying alternating current), the elimination of the vortices will take place continuously during the operation of the device. The analytically predicted phase boundaries, whose position is determined by the geometry of the patterning, provide a useful tool for designing the appropriate patterning to obtain the lowest possible vortex density for current and frequency ranges desired for specific applications. Finally, although here we limited ourselves to low-temperature superconductors, the working principle of the ratchet effect also applies to high-temperature superconductors. □

Received 22 December 1998; accepted 10 May 1999.

1. Tinkham, M. *Introduction to Superconductivity* (McGraw-Hill, New York, 1996).
2. Donaldson, G. B., Pegrum, C. M. & Bain, R. J. P. in *SQUID '85: Proc. 3rd Int. Conf. on Superconducting Quantum Devices* (eds Hahlbohm, H. D. & Lübbig, H.), 749–753 (Walter Gruyter, Berlin, 1985).
3. Clarke, J. *Superconducting Devices* (eds Ruggiero, S. T. & Rudman, D. A.) 51–100 (Academic, 1990).
4. Blatter, G., Feigelman, M. V., Geshkenbeim, V. B., Larkin, A. I. & Vinokur, V. M. Vortices in high temperature superconductors. *Rev. Mod. Phys.* **66**, 1125–1388 (1994).
5. Koch, R. H., Sun, J. Z., Foglietta, V. & Gallagher, W. J. Flux dam, a method to reduce extra low-frequency noise when a superconducting magnetometer is exposed to a magnetic field. *Appl. Phys. Lett.* **67**, 709–711 (1995).
6. Dantsker, E., Tanaka, S. & Clarke, J. High- T_c superconducting quantum interference devices with slots or holes: low $1/f$ noise in ambient magnetic fields. *Appl. Phys. Lett.* **70**, 2037–2039 (1997).
7. Magnasco, M. O. Forced thermal ratchet. *Phys. Rev. Lett.* **71**, 1477–1481 (1993).
8. Astumian, R. D. Thermodynamics and kinetics of a brownian motor. *Science* **276**, 917–922 (1997).
9. Jülicher, F., Ajdari, A. & Prost, J. Modeling molecular motors. *Rev. Mod. Phys.* **69**, 1269–1281 (1997).
10. Hänggi, P. & Bartussek, R. in *Lecture Notes in Physics* Vol. 476 (eds Parisi, J. et al.) 294–308 (Springer, Berlin, 1996).
11. Clem, J. R., Huebener, R. P. & Gallus, D. E. Gibbs free-energy barrier against irreversible magnetic flux entry into a superconductor. *J. Low Temp. Phys.* **12**, 449–477 (1973).
12. Mück, M. Practical aspects for SQUID applications. *Superlattices Microstruct.* **21**, 415–421 (1997).
13. Scott, B. A., Kirtley, J. R., Walker, D., Chen, B.-H. & Wang, Y. Application of scanning SQUID petrology to high-pressure materials science. *Nature* **389**, 164–167 (1997).
14. Rousselet, J., Salome, L., Ajdari, A. & Prost, J. Directional motion of brownian particles induced by a periodic asymmetric potential. *Nature* **370**, 446–448 (1994).
15. Faucheux, L. P., Bourdieu, L. S., Kaplan, P. D. & Libchaber, A. J. Optical thermal ratchet. *Phys. Rev. Lett.* **74**, 1504–1507 (1995).
16. Kelly, T. R., Silva, H. D. & Silva, R. A. A rationally designed molecular motor. *Nature* (submitted).
17. Derényi, I., Lee, C.-S. & Barabási, A.-L. Ratchet effect in surface electromigration: smoothing surfaces by an AC field. *Phys. Rev. Lett.* **80**, 1473–1476 (1998).
18. Zapata, I., Bartussek, R., Sols, F. & Hänggi, P. Voltage rectification by a SQUID ratchet. *Phys. Rev. Lett.* **77**, 2292–2295 (1996).

19. Zapata, I., Luczka, J., Sols, F. & Hänggi, P. Tunneling center as a source of voltage rectification in Josephson junctions. *Phys. Rev. Lett.* **80**, 829–832 (1998).
20. Reichhardt, C., Olson, C. J. & Nori, F. Nonequilibrium dynamic phases and plastic flow of driven vortex lattices in superconductors with periodic arrays of pinning sites. *Phys. Rev. B* **58**, 6534–6564 (1998).
21. Reichhardt, C., Olson, C. J. & Nori, F. Dynamic phases of vortices in superconductors with periodic pinning. *Phys. Rev. Lett.* **78**, 2648–2651 (1997).
22. Olson, C. J., Reichhardt, C. & Nori, F. Nonequilibrium dynamic phase diagram for vortex lattices. *Phys. Rev. Lett.* **81**, 3757–3760 (1998).
23. Zeldov, E. *et al.* Geometrical barriers in high-temperature superconductors. *Phys. Rev. Lett.* **73**, 1428–1431 (1994).

Acknowledgements. We thank R. D. Astumian, D. J. Bishop, S. N. Coppersmith, D. Grier, H. Jeong, A. Koshlev and S. T. Ruggiero for discussions and help during the preparation of the manuscript. This research was supported by an NSF Career Award.

Correspondence and requests for materials should be addressed to A.-L.B. (e-mail: alb@nd.edu).

Synthesis of cubic silicon nitride

Andreas Zerr^{*}, Gerhard Miehe[†], George Serghiou[‡],
 Marcus Schwarz^{*}, Edwin Kroke^{*}, Ralf Riedel^{*},
 Hartmut Fueß[†], Peter Kroll[§] & Reinhard Boehler[‡]

^{*}Fachgebiet Disperse Feststoffe, [†]Fachgebiet Strukturforchung,
 Fachbereich Materialwissenschaft, Technische Universität Darmstadt,
 Petersenstrasse 23, D-64287 Darmstadt, Germany

[‡]Max-Planck-Institut für Chemie, Postfach 3060, D-55020 Mainz, Germany

[§]Cornell University, Department of Chemistry, Baker Laboratory, Ithaca,
 New York 14853-1301, USA

Silicon nitride (Si₃N₄) is used in a variety of important technological applications. The high fracture toughness, hardness and wear resistance of Si₃N₄-based ceramics are exploited in cutting tools and anti-friction bearings¹; in electronic applications, Si₃N₄ is used as an insulating, masking and passivating material². Two polymorphs of silicon nitride are known, both of hexagonal structure: α - and β -Si₃N₄. Here we report the synthesis of a third polymorph of silicon nitride, which has a cubic spinel structure. This new phase, *c*-Si₃N₄, is formed at pressures above 15 GPa and temperatures exceeding 2,000 K, yet persists metastably in air at ambient pressure to at least 700 K. First-principles calculations of the properties of this phase suggest that the hardness of *c*-Si₃N₄ should be comparable to that of the hardest known oxide (stishovite³, a high-pressure phase of SiO₂), and significantly greater than the hardness of the two hexagonal polymorphs.

The spinel structure is found in many binary and ternary metal oxides, silicates and sulphides, such as Fe₃O₄, γ -Mg₂SiO₄ or Fe₃S₄ (ref. 4). A mixed oxide/nitride spinel phase is formed from Al₂O₃ and AlN which is known as ALON (Al₂₃O₂₇N₅; ref. 5). The highest proportion of nitrogen anions (up to 75%) is contained in another oxide/nitride spinel, Mn₂(MnTa₃)N_{6- δ} O_{2- δ} (0 \leq δ \leq 1)⁶. In oxynitride spinels, as well as in other structures such as the solid solution of Si₃N₄ and Al₃O₃N denoted as β -SiALON, the silicon atoms are coordinated to both nitrogen and oxygen. The only oxide/nitride compound containing pure SiN₆ octahedra is, to our knowledge, the nitrido silicate Ce₁₆Si₁₅O₆N₃₂, which crystallizes in a perovskite-like structure⁷. However, pure nitride-based, non-oxide solid silicon compounds containing six-fold coordinated silicon atoms have not so far been reported.

Particular interest in the high-pressure phase behaviour of Si₃N₄ arises from a theoretical prediction⁸ that the hardness of hypothetical β -C₃N₄ (with the hexagonal β -Si₃N₄ structure) may be comparable to that of diamond. It was suggested in a more recent theoretical study⁹ that cubic C₃N₄ with the structure of the high-pressure phase of Zn₂SiO₄ (willemite II, space group *I43m*) has a bulk modulus (and possibly a hardness) greater than that of diamond.

The compound α -Si₃N₄, with a density of $\rho = 3.183 \text{ g cm}^{-3}$ (ref. 10) has been synthesized at ambient pressure and temperatures

below 1,800 K, while the β -phase ($\rho = 3.200 \text{ g cm}^{-3}$ (ref. 10)) requires higher temperatures^{11,12}. The relative stability of these phases and the influence of oxygen on the stability of α -Si₃N₄ is not well understood. This subject is discussed in more detail in ref. 1. Both α - and β -Si₃N₄ maintain their structure during compression at room temperature up to 48 GPa (ref. 13) and 28 GPa (A.Z., R.B. and R.R., manuscript in preparation), respectively. The β -phase has been synthesized at 1.5 GPa and 1,400 K from silicon and nitrogen using YAG-laser heating in a diamond cell¹⁴, and from α -Si₃N₄ at \sim 5 GPa and 2,270 K using an internally heated high-pressure vessel¹². No high-temperature experiments on silicon nitride above 9 GPa have yet been performed.

To investigate the high-pressure and high-temperature phase behaviour of silicon nitride, we utilized the technique of laser heating in a diamond cell. In all experiments, silicon single crystals or cold-pressed powder pellets of amorphous Si₃N₄ and polycrystalline α - and β -Si₃N₄ were placed in a nitrogen pressure medium. Nitrogen was used for two reasons: first, for the case where silicon was used as a starting material, it served as a reactant for the synthesis of silicon nitride. Second, it precludes decomposition of silicon nitride starting materials on heating. A neodymium:yttrium-lithium-fluoride laser (Nd:YLF; Antares-YLF, Coherent, Palo Alto) was used for heating silicon, and a CO₂ laser (Melles Griot, Carlsbad, California) for heating silicon nitride. Details of the laser heating techniques, temperature measurement, and sample pressure–temperature conditions are given elsewhere^{15,16}. The starting crystalline materials were characterized by Raman spectroscopy^{11,17}. The samples were heated at constant pressure for 1–10 min and then quenched by switching off the laser power. The reaction products were examined by Raman spectroscopy at high pressure and on pressure decrease. The recovered samples were investigated using a transmission electron microscope (TEM; Philips CM20UT) equipped with an energy dispersive X-ray (EDX) detector (HPGe, Voyager, Noran Instruments, Middleton, Wisconsin). TEM and EDX analysis allowed us to determine the crystal structure, and to obtain semiquantitative information on the chemical composition.

In the first experiment, elemental silicon was heated at 5.2 GPa using the Nd:YLF laser. Above 2,100 K, temperature fluctuations indicated a chemical reaction of silicon with the nitrogen pressure

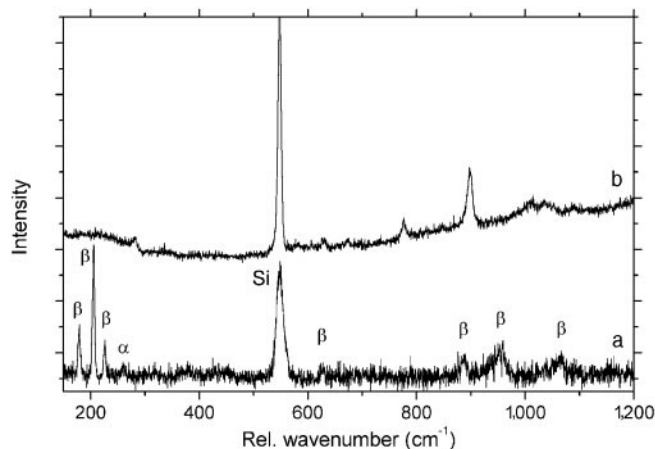


Figure 1 High-pressure Raman spectra of silicon nitride phases synthesized by heating elemental silicon and molecular nitrogen in a diamond cell. Trace a; At 5.2 GPa we found, in addition to the Raman band of silicon (labelled 'Si'), seven new lines corresponding to hexagonal β -Si₃N₄ and one new weak line that can be assigned to the most intense Raman line of hexagonal α -Si₃N₄ at this pressure. Trace b; after heating at 15 GPa none of the Raman lines obtained can be attributed to the known phases of silicon or α - or β -Si₃N₄, indicating the appearance of a new cubic silicon nitride phase with spinel-type structure (see text and Fig. 2).